Synthesis, Characterization, and Photophysical Properties of Novel BODIPY and [Zn(dipyrrin)₂] Complexes from an Asymmetrical Dipyrromethene Ligand

Gökhan Sevinç[1]* iD

[1]Bilecik Seyh Edebali University, Faculty of Science, Department of Chemistry, TR 11100 Bilecik, Turkiye.

Abstract: In this study, novel homoleptic BF_2 and Zn(II) complexes derived from an asymmetric dipyrromethene ligand were synthesized, with their chemical structures elucidated through NMR, and HRMS techniques. The photophysical characteristics in solution were investigated utilizing UV-visible absorption and fluorescence spectroscopy. The experimental results are clarified through Density Functional Theory (DFT) calculations and electron-hole analysis. Theoretical analyses have demonstrated that, following excitation, both electrons and holes remain confined exclusively within the BODIPY core. The charge-transfer transitions were identified between reciprocal ligands, which are responsible for the redshift observed in the main absorption band, as evidenced by electron-hole analysis. The energy levels of the frontier molecular orbitals converge contingent upon the incorporation of naphthyl and *p*-methoxyphenyl substituents. When analyzed under an inert nitrogen atmosphere, the compounds exhibited considerable thermal stability. Despite the similarity in the TGA curves of the complexes, the formation of the homoleptic complex resulted in an enhancement in degradation temperatures. This study indicates that chromophoric dipyrromethene complexes present advantageous prospects for advancing the development of novel materials that are both photostable and thermostable, effectively integrating charge transfer with low energy within the visible and/or near-infrared spectra.

1. INTRODUCTION

Dipyrromethene (dpm) compounds, also known as dipyrrins, represent a significant group of conjugated, bipyrrolic chelators that have gained growing interest in recent years. These compounds are organic moieties capable of coordinating with various metal atoms to form stable complex structures. Dipyrromethene-metal complexes are characterized by notable features such as photostability and thermal stability, facile chemical synthesis, and significant absorptive capacity, particularly within the visible spectrum (1–3). The π-conjugation within these bis-pyrrolic systems enhances the efficient absorption of visible light via π – π* transitions. Dipyrrins are crucial in current chemical research due to their easy synthesis, intriguing photophysical properties, and diverse self-assembled architectures. Dipyrrin compounds are particularly significant as they serve as precursors to porphyrin and dipyrromethene-BF₂ complexes known as BODIPYs (4,5). Porphyrins can be synthesized artificially and are also found in

numerous natural substances, including hemoglobin and chlorophyll (6). BODIPY (4,4-difluoro-4-bora-3a,4a-diaza-*s*-indacene) dyes (4,5,7,8) are actively researched within diverse applications such as chemical and biological sensors (9–12), two-photon absorption (13,14), dye-sensitized solar cells (15,16), and cellular imaging (17,18). This is owing to their pronounced fluorescence in the visible spectrum, distinct absorption and emission peaks, inherent stability, and adaptability to chemical modifications. Dipyrrin compounds are typically synthesized through the condensation of aromatic aldehydes and pyrroles, resulting in the formation of symmetric products. (1,3). BODIPY compounds are generally synthesized from aromatic aldehyde and pyrrole starting materials. The dipyrromethane intermediates obtained in the first stage are converted to dipyromethane ligands by oxidation in the presence of *p*-chloranil (Tetrachloro-p-benzoquinone) or DDQ (2,3-Dichloro-5,6-dicyano-1,4-benzoquinone). The complexation is completed with BF₃.OEt₂ in the presence of an organic base such as triethylamine (Scheme 1).
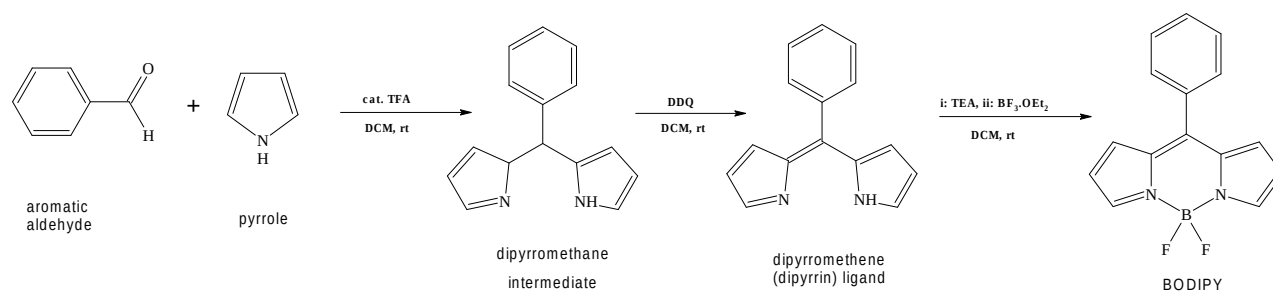
Scheme 1: The sample reaction in BODIPY synthesis from an aromatic aldehyde (benzaldehyde) and pyrrole starting materials.

The literature documents the synthesis, characterization, and diverse applications of these symmetrical dipyrrins and their corresponding metal or BODIPY complexes (1–3). Research on asymmetrically structured dipyrrins and their metal complexes, including BF$_2$, is limited (19,20). This scarcity may be due to the challenges in synthesizing asymmetrical dipyrromethenes. The asymmetric structure can be imparted via Knoevenagel reactions from alpha alkyl substituted dipyrromethene or generally BODIPY compounds. In these reactions, binary symmetric products (distyryl products) are mostly obtained. An alternative to this method, which limits the yield of response, is to use different pyrroles to obtain asymmetric dipyrromethenes. Therefore, in order to make complex purification procedures, a 1,3-dimethyl-BODIPY scaffold can be used, which can only lead to monostyryl products (19,20). Apart from this, one of the key steps in the formation of the asymmetrical dipyrrin backbone is the condensation of pyrrole carboxaldehyde and pyrrole derivatives. When the substituent groups on the pyrroles are the same, symmetric dipyrins are obtained, and when they are different, asymmetric dipyrrin ligands are obtained.

The transition metal coordination chemistry of dipyrrine ligands, which are notable for their intense absorption in the red region of the spectrum, is a current topic (1–3). Coordination of dipyrromethenes with the Zn(II) gives M(L)$_2$ type homoleptic complexes with distorted tetrahedral geometry. In this search to incorporate the hyperconjugated asymmetrical structures, Zn(II) was preferred as the metal ion of choice for comparing with the Boron (III) coordination because the closed-shell (d^{10}) configuration of Zn(II) and allowing for faster theoretical calculations. Unlike the previous studies, pyrroles containing aromatics such as phenyl and naphthyl groups at the 2,4-positions of the pyrrole were used, and thus, increased conjugation was aimed. To achieve this, two novel dyes featuring asymmetric structures were synthesized from the 2,4-diaryl-1*H*-pyrrole derivatives. The dipyrromethene framework, incorporating different aromatic groups at the -α (-1, -9) and -β (-3, -7) positions, was obtained. The structural elucidation of the compounds was conducted utilizing ^{1}H/^{13}C NMR, and HRMS techniques. The effect of the asymmetric structure and metal/semimetal coordination on the absorption and fluorescence characteristics of the compounds was ascertained. The relationships between chemical structure and photophysical properties were examined through the application of density

functional theory (DFT) calculations. In the final step, the impact of substituted groups, conjugation, and asymmetric formation on the thermal properties of the compounds was examined through thermogravimetric analysis (TGA).

2. EXPERIMENTAL SECTION

2.1. Materials and Instruments
The novel compounds **NafmetBDP** and **NafmetZn** were synthesized utilizing reagents sourced from commercial suppliers. The solvents employed in the absorption and fluorescence measurements were of spectroscopic grade. Reaction progress was monitored using thin-layer chromatography (TLC) aluminum sheets coated with silica gel (Merck 60 F254) and illuminated with a UV lamp. Column chromatography was conducted employing silica gel 60 with a mesh size of 230 - 400. High-resolution mass spectra were acquired using the Agilent 6224 LC/MS spectrometer, operating in both positive and negative modes. ^{1}H-NMR spectra were acquired using a Bruker Avance 500 MHz spectrometer in deuterated chloroform (CDCl$_3$) with tetramethylsilane (TMS) as the internal standard, whereas ^{13}C-NMR spectra were recorded at a frequency of 125 MHz in the same solvent. Chemical shifts (δ) were given in ppm relative to the solvent peaks (CDCl$_3$: ^{1}H: δ 7.26; ^{13}C: δ 77.4). The coupling constants (*J*) were reported in hertz. Thermogravimetric analysis (TGA) of the dyes was performed by heating the compounds with the Exstar SII TGA/DTA 7200 device under nitrogen flow with a heating rate of 10 °C / min in the range of 30-1100 ° C. 2,4-bis[4-methoxyphenyl]-1*H*-pyrrole and 2-[4-methoxyphenyl]-4-[1-naphthyl]-1*H*-pyrrole were synthesized following the experimental procedure outlined in Refs (21,22).

2.2. Synthesis
2.2.1. Synthesis of the compound NafmetBDP
400 µL of phosphoryl chloride was slowly added to dimethyl formamide (400 µL) at -4 °C, then stirred for 10 minutes at 0 °C. The ice bath was removed before stirring for another 10 minutes. Subsequently, the ice bath was reapplied, and 10 minutes thereafter, dichloroethane (2 mL) was introduced. Following 5 minutes of stirring, a solution of 2,4-bis[methoxyphenyl]-1*H*-pyrrole (400 mg, 1.79 mmol) in dichloroethane (10 mL) was added to the reaction mixture in a dropwise manner. After the addition, the ice bath was removed, and the mixture was refluxed for 30 minutes. The mixture cooled to room temperature; NaOAc (1.62 g, 19.7 mmol, 10 mL H$_2$O) was added,

followed by 30 minutes of reflux. The mixture was cooled to rt, and water (30 mL) was added. The organic phase was extracted with chloroform (2 x 30 mL). Evaporating the solvent under reduced pressure yielded the formylated pyrrole used without purification. The formyl pyrrole (150 mg, 0.49 mmol) and 2-[4-methoxyphenyl]-4-[1-Naphthyl]-1*H*-pyrrole (146 mg, 0.49 mmol) were dissolved in 5 mL of anhydrous dichloromethane. Phosphoryl chloride (50 mL) was added in five portions under cooling at 0 °C and stirred for 2 hours. The mixture was warmed to ambient temperature, after which 5 mL of dichloromethane was added and stirred for another hour. Water (50 mL) was added, and the mixture was extracted with chloroform (2 × 30 mL), with subsequent evaporation of the solvent under reduced pressure yielding 220 mg of crude dipyrromethene ligand. The ligand 100 mg (0.19 mmol) was dissolved in 50 mL of DCM, then N,N-diisopropylethylamine (1.0 mL) and $BF_3.OEt_2$ (1.00 mL) were added dropwise. After stirring the mixture at room temperature for 12 hours, it was neutralized with saturated $NaHCO_3$ (100 mL) and washed with water; the organic layer was then dried over Na_2SO_4, filtered, and the solvent was removed. Silica gel chromatography (eluent: $CHCl_3$) yielded **NafmetBDP** as a red powder. Yield: 64 mg (10%). ^{1}H-NMR (500 MHz, $CDCl_3$): δ[ppm]: 3.81 (s, 3H), 3.90 (s, 6H), 6.67 (s, 1H), 6.89-6.86 (m, 3H), 7.04-7.01 (dd, *J*:9.0 Hz, 4H), 7.17, (s, 1H), 7.35 (d, *J*:9.0 Hz, 2H), 7.49 (d, *J*:7.0 Hz, 1H), 7.58-7.55 (m, 3H), 7.96-7.92 (m, 2H), 7.99 (d, *J*:9.0 Hz, 2H), 8.05 (d, *J*:9.0 Hz, 2H), 8.24 (d, *J*:9.0 Hz, 1H). ^{13}C-NMR (125 MHz, $CDCl_3$) δ: 161.0, 160.8, 160.2, 158.1, 156.1, 145.5, 142.6, 139.3, 135.6, 134.6, 134.0, 132.1, 131.2, 130.0, 129.1, 128.9, 128.4, 128.3, 126.5, 126.2, 126.1, 125.8, 125.4, 125.1, 125.0, 120.8, 118.3, 114.5, 114.1, 113.9, 113.8, 55.3. HRMS (Q-TOF-ESI) m/z Calcd: 636.23960 ($C_{40}H_{31}BF_2N_2O_3$), found: 636.23846 [M]⁻, Δ = 1.79 ppm.

2.2.2. Synthesis of the compound NafmetZn
A mixture of the dipyrromethene ligand synthesized in the prior step (100 mg, 0.17 mmol) and $Zn(OAc)_2.2H_2O$ (25 mg, 0.11 mmol) was dissolved in n-butanol (15 mL) and subjected to stirring at 120 °C for a duration of 4 hours. After cooling to room temperature, the reaction mixture was filtered, and the resulting blue solid was washed with 10 mL of cold EtOH and then dried in vacuum. Blue-Brown solid, yield: 152 mg (72%). ^{1}H-NMR (500 MHz, $CDCl_3$): δ[ppm]: 3.52 (s, 6H), 3.71 (s, 6H), 3.82 (s, 6H), 6.40 (s, 2H), 6.58 (s, 2H), 6.74-6.69 (m, 12H), 7.02 (s, 2H), 7.16-7.15 (m, 4H), 7.66-7.41 (m, 16H), 7.87 (d, *J*:8.5 Hz, 2H), 7.96 (d, *J*:8.0 Hz, 2H). ^{13}C-NMR (125 MHz, $CDCl_3$) δ: 159.6, 158.8, 133.9, 133.7, 132.4, 130.1, 128.6, 128.5, 128.3, 128.2, 127.9, 127.7, 126.9, 126.1, 125.7, 117.7, 115.3, 113.6, 113.3, 113.2, 55.3, 55.2, 55.1. HRMS (Q-TOF-ESI) m/z Calcd: 1238.39612 ($C_{80}H_{62}N_4O_6Zn$), found: 1239.39946 [M+H]⁺, Δ = 2.81 ppm.

2.3. Photophysical Measurements
Compounds were initially dissolved in chloroform; after evaporation, final solutions at 1.0×10^{-5} M

concentration were achieved by adding THF. The steady-state UV-vis spectra of the compounds were recorded on a Shimadzu UV-1800 scanning spectrophotometer, while the fluorescence spectra were measured on a Perkin Elmer LS55 spectrophotometer. In fluorescence measurements conducted at 25 °C, a 1 cm quartz cell was used with the excitation and emission slit intervals set to 10.0 nm and 8.0 nm, respectively. Baseline corrected UV-vis spectra were collected from 200 to 1100 nm, and fluorescence spectra from 200 to 900 nm. The BODIPY dyes were excited at the wavelengths of maximum UV-vis absorption. Fluorescence quantum (Φ_F) yields were calculated using equation 1, with Rhodamine B (Φ_F=0.70 in ethanol) as the reference (23,24).

$$\Phi_F = \Phi_F(Std) \frac{F.A_{Std}.n^2}{F_{Std}.A.n_{Std}^2}$$

(1)

In the equation: Φ_F is the quantum efficiency of the sample; Φ_F (Std) is the reference's quantum yield; F and F_{Std} are the areas under the fluorescence emission curves for the sample and standard, respectively; A and A_{Std} are absorbance values at the excitation wavelength for the sample and standard; n and n_{Std} are the refractive indices of the solvents for the sample and standard.

2.4. DFT Calculations
Ground state geometric optimizations and excited state calculations were conducted using Density Functional Theory (DFT) and time-dependent DFT (TDDFT). These methods provided results that were consistent with experimental data reported in the literature (25–27). Computational calculations and visualizations regarding the compounds were executed utilizing Gaussian 09 Rev. C.01 and GaussView 5.0.9, respectively (28). The hybrid B3LYP functional with a mixed basis set was used to optimize molecular geometries. 6-311G was applied to **NafmetBDP**, and LANL2DZ to **NafmetZn** in the ground state at the gas phase. Frequency analysis confirmed optimised structures as true energy minima. TDDFT calculated the dyes' excited-state properties using the same functional and basis set as for the ground state. The keyword *IOp (9/40=4)* was employed to improve the precision of configuration coefficients in TDDFT calculations. Natural transition orbitals (NTOs) and hole-electron analysis of the final compounds were obtained from the transition density matrices and first excited-state energies, respectively, using TDDFT calculations with Multiwfn (29).

3. RESULTS AND DISCUSSION

3.1. Synthesis and Characterization
The asymmetrical complexes (**NafmetBDP** and **NafmetZn**) were synthesized through a series of procedural steps, as depicted in Scheme 2.
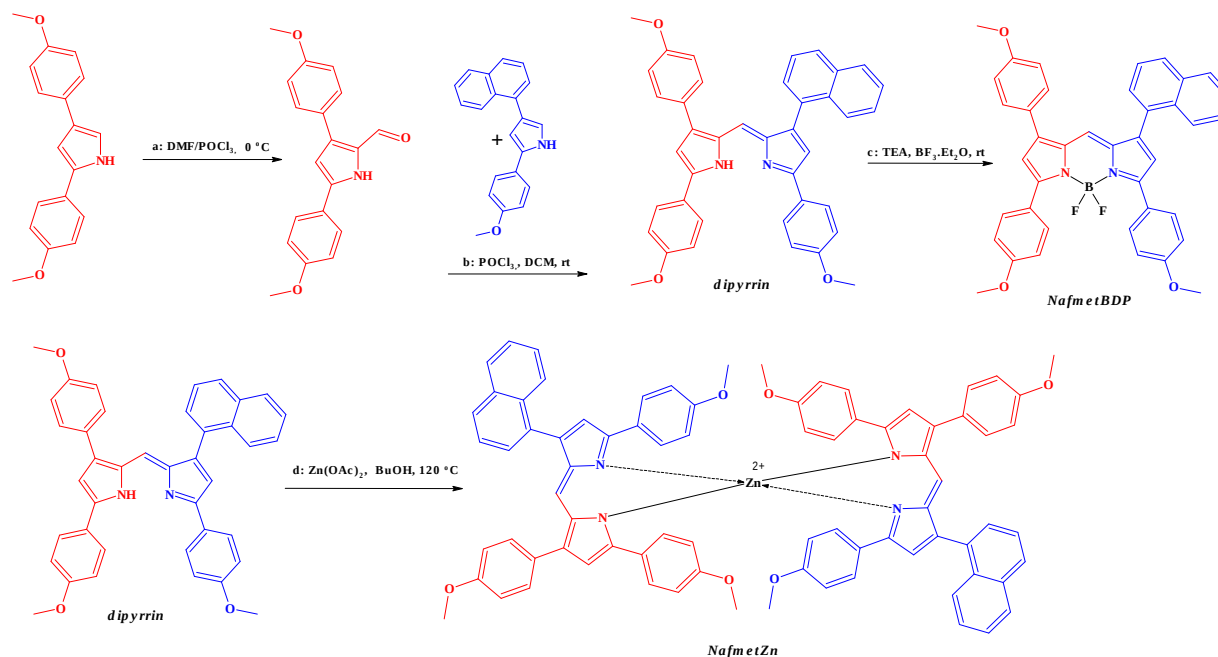
Scheme 2: The synthesis of the target molecules.

The individual preparation methodologies of these compounds are documented in literature and are conducted under mild conditions, yielding moderate synthesis efficiency (4). Initially, the precursor 2,4-bis(methoxyphenyl)-1*H*-pyrrole underwent formylation via the Vilsmeier-Haack reaction. Subsequently, the ultimate product was synthesized through acid-catalyzed condensation with a secondary pyrrole compound (2-methoxy-4-naphthyl-1*H*-pyrrole), resulting in the formation of an asymmetric dipyrromethene structure. Partitioned into two fractions, the initially isolated crude product facilitated the synthesis of BODIPY using BF₃.OEt₂, and a Zinc(II) complex was subsequently prepared to form a homoleptic complex utilizing Zinc(II) acetate salt. The BODIPY compound was subjected to purification via column chromatography, whereas the Zinc(II) complex underwent purification through cold precipitation in the butanol reaction solvent. The characterizations were conducted using ^{1}H/^{13}C NMR and HRMS analysis, confirming the data matched the expected structures. The ^{1}H-NMR measurements of the resulting compounds gave well-resolved spectra in the typical range of 0–9 ppm. The protons in aromatic groups gave singlet or distinct multiplets in the range of 6.67-8.25 ppm, depending on coupling. The pyrrole hydrogen atoms located at the -2 and -6 positions of the BODIPY core in **NafmetBDP** were identified as two separate singlet peaks at 6.67 ppm and 6.89 ppm, respectively. In contrast, the hydrogen atom at the *meso* (8) position exhibited a singlet peak at 7.17 ppm. This observation aligns with the inherent asymmetrical attributes of the structure. Furthermore, the methoxy (-OCH3) hydrogens are situated in the -α (-

3, -5) and -β (-1, -7) positions in the BODIPY core exhibit two distinct chemical shifts. Even though the structure contains three methoxy groups, the ones located at the -α position gave a singlet peak at 3.90 ppm corresponding to six hydrogen atoms (Fig. 1a). The hydrogens belonging to the methoxy groups in the alpha position of the structure were observed as a singlet peak at 3.81 ppm (Fig. 1a). This shows that the methoxy hydrogens at distant core positions have limited influence on the chemical environment, despite the structure's asymmetry. This indicates that the distant methoxy hydrogens in the asymmetric structure minimally affect the chemical environment. In the **NafmetZn**, the aforementioned methoxy peaks were detected as three singlets at 3.82, 3.71, and 3.52 ppm, as expected (Fig. 1b). The methoxy protons located adjacent to the Zn coordination center (-α positions) displayed broadened peaks, a phenomenon attributed to the Zn central atom's fully occupied d^{10} electronic configuration. In contrast, the protons positioned at the -β positions of the structure were characterized by distinct sharp singlets (Fig. 1b). In the **NafmetZn**, it was ascertained that the observed spectral peaks, primarily comprising multiplets, were in agreement with the hydrogen numbers. The differentiation of methoxy carbons, which are highly specific within these compounds, was evident in the ^{13}C NMR spectra and mirrored in ^{1}H NMR. The differentiation of methoxy carbons was apparent in the **NafmetZn** complex, identified at 55.3, 55.2, and 55.1 ppm (Fig. 1d), whereas in the BODIPY analog, the corresponding carbons exhibited overlapping signals (Fig. 1c). The carbon numbers in the compounds match the natural asymmetric structures of the compounds.
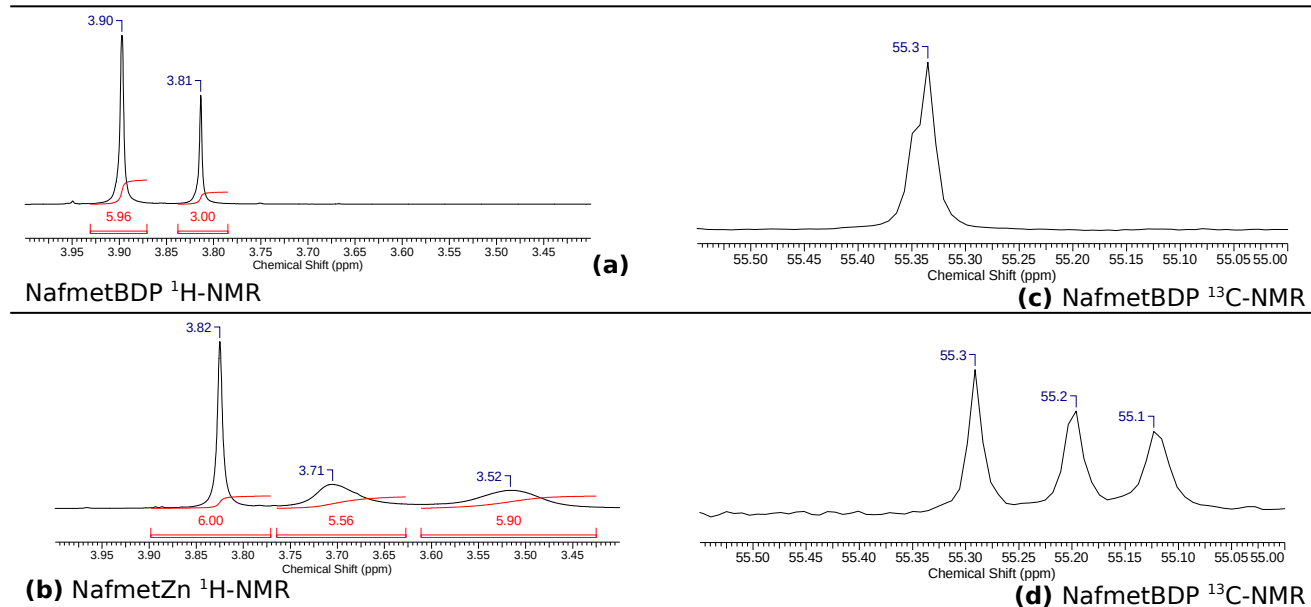
Figure 1: The scale of chemical shifts for NafmetBDP and NafmetZn for methoxy group peaks in ^{1}H-NMR (left) and ^{13}C-NMR (right).

Employing the ESI-TOF methodology, high-resolution mass spectra (HRMS) were acquired, and theoretical molecular masses were computed with consideration of isotopic contributions. The respective peaks were identified as the molecular ion peaks [M]$^-$ for **NafmetBDP** and [M+H]$^+$ for **NafmetZn**. The deviations in mass accuracy, expressed in parts per million (ppm, Δ), were ascertained to be 1.79 and 2.81 for the mentioned compounds, respectively. The HRMS/TOF data

substantiated that the experimentally observed structures corresponded with their theoretical values.

3.2. Photophysical Properties
The absorption and fluorescence spectra of the compounds in THF at room temperature were obtained. The related spectra of the dyes are shown in Figure 2a-b, with photophysical data in Table 1.
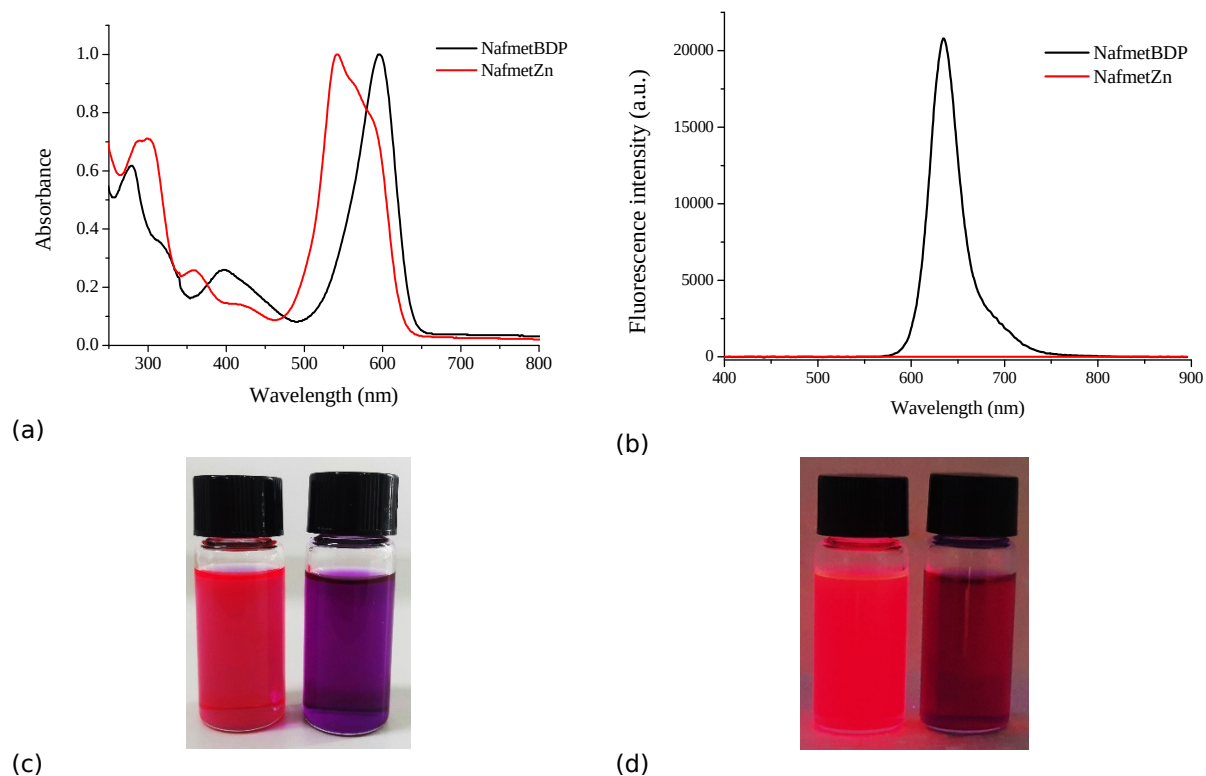

Figure 2: (a) Normalised absorption and (b) fluorescence spectra of the dyes **NafmetBDP** (λ$_{exc}$: 597 nm, slit 10.0 nm; λ$_{ems}$: 635 nm, slit 8.0 nm) and **NafmetZn** (λ$_{exc}$: 542 nm, slit 10.0 nm; ems slit 8.0 nm) in 1x10^{-6} M THF (c) The samples of **NafmetBDP** and **NafmetZn** solutions in THF under ambient light and (d) under UV illumination (λ$_{exc}$:365 nm). From left to right, **NafmetBDP** and **NafmetZn**.

The absorption spectrum of **NafmetBDP**, characterized as a BODIPY dye, exhibited a prominent absorption band at 597 nm, corresponding to the S_0-S_1 (π-π^*) transition. Broader and less intense absorption bands within the 250-500 nm range, ascribed to the presence of substituted naphthyl and methoxy phenyl groups, correspond to transitions to higher energy states of S_0-S_2 and S_0-S_3. The shoulder attributed to the 0−1 vibrational transition associated with the main transition (S_0-S_1) in the high-energy region of the primary absorption band, typically observed in classical alkyl-substituted BODIPY compounds (4,30), was absent in this material. The full width at half maximum (FWHM) of the absorption band, covering the range of 500-650 nm, has substantially increased due to the presence of conjugated aryl substituents. The BODIPY fluorescence spectra display a single band from 580 nm to 730 nm when excited at the wavelength of maximum absorption, notably mirroring the absorption spectra. Upon excitation, the compound exhibits a pronounced emission at 635 nm, accompanied by a Stokes shift of 38 nm. The Stokes shift of the Boron complex (**NafmetBDP**) is greater compared to classical alkyl-substituted BODIPYs (4,30)—the emission peak exhibits broadening similar to that of the absorption peak. The **NafmetZn** complex gives a main absorption at 542 nm along with a shoulder at 586 nm. The absorption intensities at higher energy levels, specifically within the 250-350 nm range, showed an enhancement, which is concomitant with the augmentation in the number of aromatic substituents. The spectral bandwidth expanded from 61 nm to 81 nm, while the absorption coefficient elevated from 75400 to 89260 when compared to **NafmetBDP**. The molar absorption coefficients of the complexes are sufficiently high at the maximum of the $S_0 \rightarrow S_1$ electronic transition band, rendering them comparable to structurally analogous BODIPYs. The Zinc(II) complex does not exhibit fluorescence regardless of the excitation wavelength. The observed fluorescence quenching may be attributed to the presence of aryl substituents at the -α and -β positions. The free rotation of the substituents enhances the probability of nonradiative transitions, thereby resulting in considerable fluorescence quenching of the complexes (22). According to literature on dipyrromethene-zinc complexes, the shoulder observed in the main absorption band is attributed to charge transfer transitions (31–33). The lower absorption band identified within the main absorption band in the experimental UV-Vis spectrum of **NafmetZn** may appear to correspond to the charge transfer transitions between reciprocal ligands.

Table 1: Experimental and theoretical photophysical parameters of the compounds.

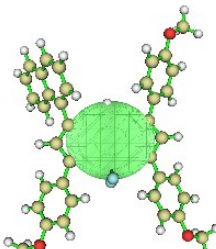| Comp.	abs (max/nm)	ems (max/nm)	$(M^{-1}cm^{-1})$	FWHM Abs / ems (nm)	Stokes shift (nm)	$^a\Phi_F$	Electronic transition	Vertical excitation energy eV/nm	Oscillator Strength f	Major Contribution
			Experimental					*DFT calculation*		
NafmetBDP	597	635	75400	61 / 37	38	0.61	$S_0 \rightarrow S_1$ $S_0 \rightarrow S_2$ $S_0 \rightarrow S_3$	2.17 / 571 2.53 / 490 2.65 / 468	0.91 0.05 0.32	H → L (99%) H-1 → L (98%) H-2 → L (98%)
NafmetZn	542	-	89260	87 / -	-	<0.001	$S_0 \rightarrow S_1$	1.92 / 647	<0.01	H-1 → L (48%), H-1 → L+1 (36%), H → L (8%), H → L+1 (8%)
							$S_0 \rightarrow S_2$	2.27 / 546	0.71	H-1 → L+1 (44%), H → L (42%), H → L+1 (10%)
							$S_0 \rightarrow S_3$	2.29 / 540	0.76	H-1 → L (41%), H → L+1 (40%), H -1→ L+1 (12%)
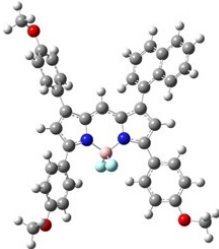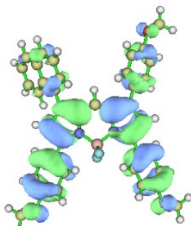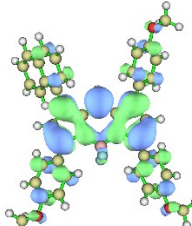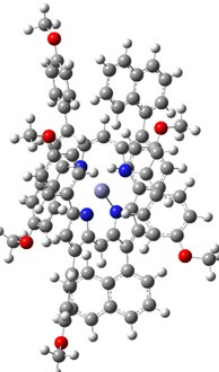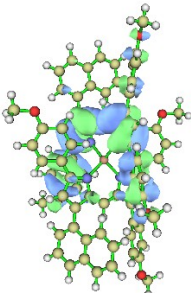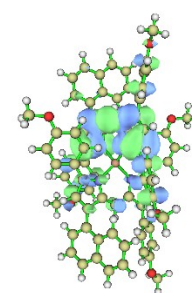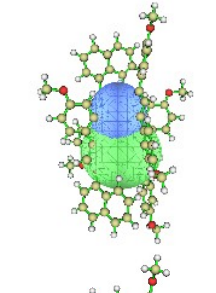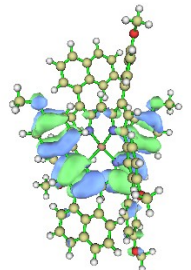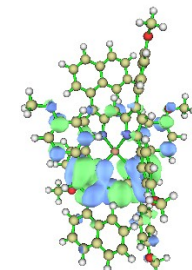
a: Rhodamine B in ethanol (Φ_F =0.70) was used as the fluorescence standard for fluorescence quantum yield calculations, and correction for the solvent refractive index (η) was applied [THF: η = 1.4072, EtOH: 1.3614].

The proximal arrangement of aryl groups at the -α and -β positions of the dipyrrin core resulted substantial bathochromic shift of the main absorption band. Beyond the π - π^* transitions stemming from the naphthyl group, the n - π^* transitions in methoxyphenyl subunits enhance the shifting. The substituent at the meso (8) position induces steric hindrance in the BODIPY core, thereby impeding the conjugation of distal aryl groups. Its absence results in the shift of BODIPY absorbance from the typical range of 500-550 nm to approximately 600 nm.
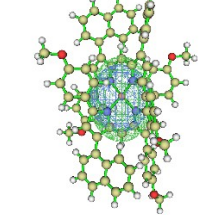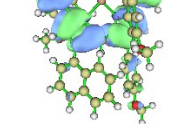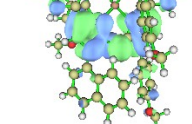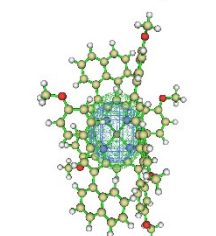
The Density Functional Theory (DFT) method has been extensively employed to elucidate the photophysical characteristics of BODIPY dyes, as it gives consistent results with the experimental findings (26,27,34). Therefore, to explain the photophysical properties of the compounds analyzed, we conducted calculations utilizing DFT/TD-DFT methods. The theoretical data that include dipole moments (μ), the electronic excitation energies (E_v), corresponding oscillator strengths (f), and the main configurations are summarized in Table 1. The optimized structures, natural transition orbitals (NTOs), and centroids of hole/electron (C_{hole} & C_{ele}) are demonstrated in Table 2.

Table 2: Optimized structures, Natural transition orbitals (NTOs) for the lowest-energy transitions (S_0-S_1) of the compounds (isosurface value = 0.02 au), centroids of hole and electron (C_{hole} & C_{ele}, isosurface value = 0.0003 au).

Comp.	Transition	Optimized structure	NTOs		C_{hole} & C_{ele}
			Electron	Hole	
NafmetBDP	Dipole moment (μ): 5.99 Debye S_0-S_1 E_E : 2.17 eV t (Å): -1.683 E_C: 3.66 eV				
NafmetZn	Dipole moment (μ): 1.42 Debye S_0-S_1: E_E :1.92 eV t (Å): 1.049 E_C: 2.87 eV				
	S_0-S_2 E_E : 2.27 eV t (Å): -2.586 E_C: 3.09 eV				
	S_0-S_3 E_E :2.29 eV t (Å): -2.502 E_C: 2.87 eV				

Blue and green isosurfaces represent C_{hole} and C_{ele} functions, respectively. *E_E* and *Ec represent the excitation energy and the Coulomb attractive energy, respectively.* The *t*-index quantifies the extent of separation between the hole and electron along the charge transfer direction.

Geometry optimizations revealed that the Borondipyrromethene core in **NafmetBDP** assumes a planar geometric configuration, while the complexes exhibit a pseudo-tetrahedral geometry. The angles formed between the F-B-F atoms and the N-B-N atoms are calculated to be 109.3° and 109.4°, respectively. The dihedral angles between the BODIPY moiety and the naphthyl and methoxyphenyl groups at the distal (1,7) positions were determined to be 52.8º and 39.94º, respectively. The dihedral angles between the methoxyphenyl groups in the proximal (3,5) positions of the compound and the dipyrrin core were determined to be 36.5º. The influence of steric hindrance exerted by the naphthyl group results in a reduction of the angle at the distal positions. Consequently, this enhances the π-π interactions between the aromatic structures situated at the proximal positions and the planar core framework. Consequently, it can be inferred that the proximal positions exert a more pronounced bathochromic effect on the photophysical characteristics of the compound. In the Zn (II) complex, the dihedral angles of the naphthyl-dipyrrine entities increased from 52.8° to 68.2°, whereas the angles involving the methoxyphenyl substituents exhibited minimal alteration. The most significant modification was observed at the proximal (3,5) positions, where the angle decreased from 36.5° to 19.9°. The formation of a stable homoleptic complex with the Zinc(II) ion between the two macrostructures was facilitated by adjusting the angles to achieve values approaching linearity.

Also, the complexes have polar character, and the dipole moments were 5.99 and 1.42 Debye for the **NafmetBDP** and **NafmetZn**, respectively. The molecular dipole moments were oriented at approximately 45° from the dipyrrin core towards the exterior of the molecules. The tetrahedral configuration of the two identical ligands in the **NafmetZn** resulted in a reduction of the dipole moment, which aligns with theoretical predictions.

The main transition in BODIPY (**NafmetBDP**) occurs between HOMO→LUMO (99% contribution) due to electronic excitations from the S_0-S_1 energy levels (Table 1), while in the **NafmetZn**, absorption processes also involve the HOMO-1 and LUMO+1 orbitals. The calculated energy band gaps ($\Delta E = |E_{HOMO} - E_{LUMO}|$) for the compounds were found to be 2.17 eV and 2.27 eV, respectively, aligning well with experimental data. It should be noted that the main transition calculated for the Zinc(II) complex exhibits a low oscillator strength (<0.01) and does not constitute a band maximum. The main transition corresponds to the S_0-S_2 transition (f: 0.71) as indicated in Table 1. The singlet excitation energies (E_E) calculated by the TDDFT method for absorption spectra (λ_{cal}) validated the experimental values (λ_{exp}), with $\lambda_{exp}/\lambda_{cal}$ ratios of 1.05 and 0.99 for **NafmetBDP** and **NafmetZn**, respectively (Figure S1.).

Natural transition orbitals (NTOs) were calculated to visualize electronic transitions, representing excited electron-hole pairs from transition density matrices via TDDFT. Table 2 lists the NTOs and centroids of hole/electron isosurfaces for the singlet transitions of the dyes. The detailed isosurfaces of all singlet transitions belonging to **NafmetBDP** are given in supplementary material. Within the NTO isosurfaces, the main distribution regions for the electron and hole are denoted by green and blue, respectively. The calculations indicate that the distribution of excited electrons and holes across the molecule constitutes the main S_0-S_1 transition. The transition occurs without the involvement of charge transfer (CT), and is predominantly localized on the BODIPY core (Table 2, C_{hole} & C_{ele}, isosurface). However, it was determined that during high-energy transitions (S_0-S_2, S_0-S_3), a net charge separation (t>0) occurred from the BODIPY core to distal positions. The electrons for the transitions were

exclusively localized on the dipyrrin skeleton, while the holes were partially spread on the substituents at the -1, -3, -5, -7, and -8 (*meso*) positions. The centroids of the hole and electron, denoted as C_{hole}/C_{ele}, facilitated the smoothness of the electron/hole distribution behavior as outlined in Table 2. There is a significant overlap between the electron and hole pairs for the S_0-S_1 transition in **NafmetBDP**.

Notably, in the low-energy S_0-S_1 transition (E_E: 1.92 eV) of the **NafmetZn**, the two ligands exhibit charge separation manifesting as electrons and holes. In this context, Zinc(II) functions as a connecting entity between the opposing ligands, facilitating a charge transfer process. In the main transitions of this complex (characterized by elevated Oscillator Strength values of f: 0.71 and 0.76, respectively), S_0-S_2 and S_0-S_3, the negative t index indicates the absence of charge separation, demonstrating that the pertinent transitions are not charge transfers. Instead, these are locally excited electronic transitions originating from dipyrrin groups. The both complexes exhibited higher Coulomb attractive energies (E_c, exciton binding energies), reducing exciton dissociation compared to transition energies (E_E).

3.3. Thermal Properties
A significant attribute of the dyes applicable to technical fields is the range of temperatures at which these compounds maintain thermal stability and exhibit no alterations in their spectral properties. Therefore, the thermal properties of the compounds were determined in an inert N_2 atmosphere utilizing thermogravimetric analysis (TGA). The thermal stability of the compounds has been characterized through a variety of quantifiable metrics. Figure 3 presents the thermal degradation graphs of the compounds, while Table 3 provides the associated thermogram parameters.

Table 3: The decomposition temperatures and thermal stability of the compounds.

Compound	T_{max} (°C)*	Mass loss (%)	Decomposition rate (%/min)	**T10% (°C)	T30% (°C)	T50% (°C)
NafmetBDP	200	17	2.11	164	286	426
	360	41	2.96			
	590	70	2.37			
	760	97	1.42			
NafmetZn	447	10	0.97	440	665	890
	878	48	1.27			
	947	57	1.86			
	994	67	2.39			

*Maximum decomposition temperatures based on DTG plot. ** T10% (the temperature at which 10% of the initial mass is lost), etc.
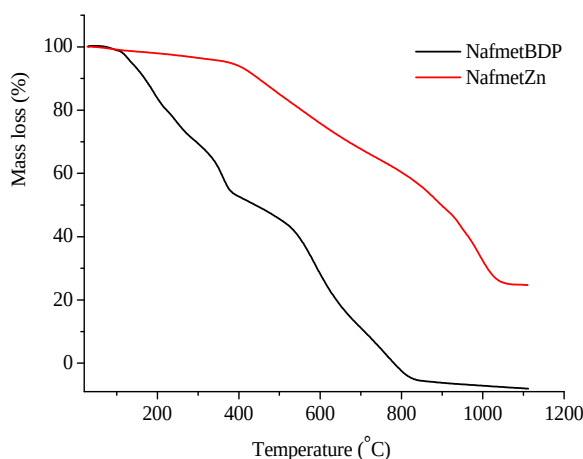
Figure 3: TGA thermogram of the compounds at a temperature ramp of 10 °C/min under N_2.

The thermal degradation of compounds, similar to that of other dipyrromethene dyes, occurs as a result of intramolecular oxidation-reduction reactions (35). The thermal destruction processes of the **NafmetBDP** and **NafmetZn** occurred in four stages, as evidenced by the TG curves displaying phases of sample weight loss. **NafmetBDP** underwent primary decomposition at 200 °C in an inert N_2 atmosphere, while the Zinc(II) complex (**NafmetZn**) began to decompose at a higher temperature of 447 °C. The most rapid degradation of the BODIPY derivative was observed in the second phase at 360 °C. Hence, it can be inferred that the thermal stability of the metal complex is considerably elevated despite the presence of identical organic substituents. Between 200-900 °C, the degradation phases showed reduced rates and mass loss, likely due to the breaking of covalent bonds and the carbonization of organic groups in the dipyrromethene framework. It should be noted that even at 994 °C, representing the final stage of decomposition, 33% of the structure of the Zn(II) complex persisted. The decomposition rates (%/min) of the BODIPY derivative are considerably greater, almost by two orders of magnitude, in comparison to those of the Zinc(II) complex. Utilizing T10% temperatures as a comparison basis, it is observed that **NafmetBDP** decomposes at 164 °C and **NafmetZn** at 440 °C, indicating that **NafmetZn** exhibits nearly threefold greater thermal stability. The carbonization efficiencies at 700 °C, generally regarded as a reference point, are 89% for **NafmetBDP** and 33% for **NafmetZn**, respectively. The coordination of homoleptic metal with an identical ligand resulted in an enhancement of the thermal stability of the dipyrromethene core when compared to its coordination with Borondifluoride (BF_2). The comparatively reduced thermal stability of BODIPY relative to Zinc(II) dipyrromethene might be attributed to the involvement of fluorine atoms in intramolecular redox processes. The residue observed at elevated temperatures in the thermogram of the compound **NafmetZn** may be due to lower oxidation potential of Zinc atoms in contrast to the substantially higher oxidation potential of fluorine atoms and the strong covalent nature of B–F bonds (36,37). Consequently, the formation of ZnO and carbonized products may occur, given that the analysis was conducted under a nitrogen atmosphere. The incorporation of aryl groups into pyrrole moieties has been found to significantly influence the thermal stability of Zinc (II) dipyrromethenates when compared to their alkyl-substituted counterparts as reported in the literature (35).

4. CONCLUSION

In summary, novel homoleptic BODIPY and [Zn(dipyrrin)$_2$] complexes were synthesized from an asymmetric dipyrromethene ligand, with structures confirmed by NMR and HRMS. Their photophysical properties in solution were examined using UV-visible absorption and fluorescence spectroscopy. The absorption band's FWHM from 500-650 nm significantly increased due to conjugated aryl substituents. While the BODIPY fluorescence spectra display a single band from 580 to 730 nm, similar to the absorption spectra at the maximum absorption wavelength, the Zinc(II) complex does not fluoresce at any excitation wavelength. Aryl groups positioned at the -α and -β sites of the dipyrrin core cause a significant bathochromic shift in the main absorption band. The shift is further enhanced by n - π* transitions in methoxyphenyl subunits and π - π* transitions from the naphthyl group, extending BODIPY absorbance from the typical range of 500-550 nm to ca. 600 nm. Density Functional Theory (DFT) calculations and electron-hole analysis reveal that the complexes have a pseudo-tetrahedral geometry and polar character. The calculations show that the main S_0-S_1 transition involves the distribution of excited electrons and holes across the molecule, and it is mainly localized on the BODIPY core without charge transfer in **NafmetBDP**. During high-energy transitions, charge separation occurs from the dipyrrin core to distant positions, with electrons localized on the

dipyrrin skeleton and holes spread on the substituents at the -1, -3, -5, -7, and -8 positions. In **NafmetZn** complex, charge-transfer transitions between reciprocal ligands cause the main absorption band's redshift, as shown by electron-hole analysis. The proximal positions significantly enhance the bathochromic effect on the compounds' photophysical properties. According to TGA, the coordination of Zinc(II) resulted in considerable thermal stability and enhanced degradation temperatures. **NafmetZn** demonstrates a thermal stability that is nearly three times greater than BODIPY analogue. Aryl groups in pyrrole moieties significantly enhanced the thermal stability of Zinc(II) dipyromethenates compared to their alkyl counterparts. This work shows that chromophoric dipyrromethene complexes hold promise for developing photostable and thermostable materials capable of energy transfer in the visible spectra.

5. CONFLICT OF INTEREST

The author declares no competing interests.

6. ACKNOWLEDGMENTS

7. REFERENCES

1. Wood TE, Thompson A. Advances in the chemistry of dipyrrins and their complexes. Chem Rev [Internet]. 2007 May 1;107(5):1831–61. Available from: <URL>.

2. Baudron SA. Dipyrrin based metal complexes: reactivity and catalysis. Dalt Trans [Internet]. 2020 May 19;49(19):6161–75. Available from: <URL>.

3. Shikha Singh R, Prasad Paitandi R, Kumar Gupta R, Shankar Pandey D. Recent developments in metal dipyrrin complexes: Design, synthesis, and applications. Coord Chem Rev [Internet]. 2020 Jul 1;414:213269. Available from: <URL>.

4. Loudet A, Burgess K. BODIPY dyes and their derivatives: Syntheses and spectroscopic properties. Chem Rev [Internet]. 2007 Nov 1;107(11):4891–932. Available from: <URL>.

5. Lu H, Shen Z. BODIPYs and their derivatives: The past, present and future. Front Chem [Internet]. 2020 Apr 28;8:541725. Available from: <URL>.

6. Tahoun M, Gee CT, McCoy VE, Sander PM, Müller CE. Chemistry of porphyrins in fossil plants and animals. RSC Adv [Internet]. 2021 Feb 17;11(13):7552–63. Available from: <URL>.

7. M. Ravikanth M, Vellanki L, Sharma R. Functionalized boron-dipyrromethenes and their applications. Reports Org Chem [Internet]. 2016 Jan;6:1–24. Available from: <URL>.

8. Yilmaz RF, Derin Y, Misir BA, Atalay VE, Tutar ÖF, Ökten S, et al. Synthesis and spectral properties of symmetrically arylated BODIPY dyes: Experimental and computational approach. J Mol Struct [Internet]. 2023 Nov 5;1291:135962. Available from: <URL>.

9. Wang L, Ding H, Ran X, Tang H, Cao D. Recent progress on reaction-based BODIPY probes for anion detection. Dye Pigment [Internet]. 2020 Jan 1;172:107857. Available from: <URL>.

10. Bumagina NA, Antina E V. Review of advances in development of fluorescent BODIPY probes (chemosensors and chemodosimeters) for cation recognition. Coord Chem Rev [Internet]. 2024 Apr 15;505:215688. Available from: <URL>.

11. Nuri Kursunlu A, Guler E. The sensitivity and selectivity properties of a fluorescence sensor based on quinoline-Bodipy. J Lumin [Internet]. 2014 Jan 1;145:608–14. Available from: <URL>.

12. Boens N, Leen V, Dehaen W. Fluorescent indicators based on BODIPY. Chem Soc Rev [Internet]. 2012 Jan 17;41(3):1130–72. Available from: <URL>.

13. Yang J, Jiang H, Desbois N, Zhu G, Gros CP, Fang Y, et al. Synthesis, spectroscopic characterization, one and two-photon absorption properties, and electrochemistry of truxene π-expanded BODIPYs dyes. Dye Pigment [Internet]. 2020 May 1;176:108183. Available from: <URL>.

14. Song G, Li Z, Han Y, Jia J, Zhou W, Zhang X, et al. Enhancement of two-photon absorption in boron-dipyrromethene (BODIPY) Derivatives. Molecules [Internet]. 2022 Apr 29;27(9):2849. Available from: <URL>.

15. Klfout H, Stewart A, Elkhalifa M, He H. BODIPYs for dye-sensitized solar cells. ACS Appl Mater Interfaces [Internet]. 2017 Nov 22;9(46):39873–89. Available from: <URL>.

16. Singh SP, Gayathri T. Evolution of BODIPY dyes as potential sensitizers for dye-sensitized solar cells. European J Org Chem [Internet]. 2014 Aug 16;2014(22):4689–707. Available from: <URL>.

17. Kaur P, Singh K. Recent advances in the application of BODIPY in bioimaging and chemosensing. J Mater Chem C [Internet]. 2019 Sep 26;7(37):11361–405. Available from: <URL>.

18. Kolemen S, Akkaya EU. Reaction-based BODIPY probes for selective bio-imaging. Coord Chem Rev [Internet]. 2018 Jan 1;354:121–34. Available from: <URL>.

19. Ono M, Watanabe H, Kimura H, Saji H. BODIPY-based molecular probe for imaging of cerebral β-amyloid plaques. ACS Chem Neurosci [Internet]. 2012 Apr 18;3(4):319–24. Available from: <URL>.

20. Lee JS, Kang N young, Kim YK, Samanta A, Feng S, Kim HK, et al. Synthesis of a BODIPY library and its application to the development of live cell glucagon imaging probe. J Am Chem Soc [Internet]. 2009 Jul 29;131(29):10077–82. Available from: <URL>.

21. Gawley RE, Mao H, Haque MM, Thorne JB, Pharr JS. Visible fluorescence chemosensor for saxitoxin. J Org Chem [Internet]. 2007 Mar 1;72(6):2187–91. Available from: <URL>.

22. Sevinç G, Küçüköz B, Elmalı A, Hayvalı M. The synthesis of −1, −3, −5, −7, −8 aryl substituted boron-dipyrromethene chromophores: Nonlinear optical and photophysical characterization. J Mol Struct [Internet]. 2020 Apr 15;1206:127691. Available from: <URL>.

23. Bittel AM, Davis AM, Wang L, Nederlof MA, Escobedo JO, Strongin RM, et al. Varied length stokes shift BODIPY-based fluorophores for multicolor microscopy. Sci Rep [Internet]. 2018 Mar 15;8(1):4590. Available from: <URL>.

24. Kubin RF, Fletcher AN. Fluorescence quantum yields of some rhodamine dyes. J Lumin [Internet]. 1982 Dec 1;27(4):455–62. Available from: <URL>.

25. Emirik M, Karaoğlu K, Serbest K, Çoruh U, Vazquez Lopez EM. Two novel unsymmetrical ferrocene based azines and their complexing abilities towards Cu(II): Spectroscopy, crystal structure, electrochemistry and DFT calculations. Polyhedron [Internet]. 2015 Mar 9;88:182–9. Available from: <URL>.

26. Laine M, Barbosa NA, Wieczorek R, Melnikov MY, Filarowski A. Calculations of BODIPY dyes in the ground and excited states using the M06-2X and PBE0 functionals. J Mol Model [Internet]. 2016 Nov 7;22(11):260. Available from: <URL>.

27. Matveeva MD, Zheleznova TY, Kostyuchenko AS, Miftyakhova AR, Zhilyaev DI, Voskressensky LG, et al. 1,7-isoxazolyl substituted BODIPY dyes – synthesis and photophysical properties. ChemistrySelect [Internet]. 2023 Feb 3;8(5):e202204465. Available from: <URL>.

28. Frisch R, Trucks GW, Schlegel HB, Scuseria GE, Robb MA, Cheeseman JR. Gaussian09, 1 121, gaussian. 2009;150–66.

29. Lu T, Chen F. Multiwfn: A multifunctional wavefunction analyzer. J Comput Chem [Internet]. 2012 Feb 15;33(5):580–92. Available from: <URL>.

30. Sevinç G, Küçüköz B, Yılmaz H, Şirikçi G, Yaglioglu HG, Hayvalı M, et al. Explanation of pH probe mechanism in borondipyrromethene-benzimidazole compound using ultrafast spectroscopy technique. Sensors Actuators B Chem [Internet]. 2014 Mar 31;193:737–44. Available from: <URL>.

31. Akhüseyin E, Türkmen O, Küçüköz B, Yılmaz H, Karatay A, Sevinç G, et al. Two photon absorption properties of four coordinated transition metal complexes of tetraarylazadipyrromethene compounds. Phys Chem Chem Phys [Internet]. 2016 Feb 3;18(6):4451–9. Available from: <URL>.

32. Teets TS, Partyka D V., Updegraff JB, Gray TG. Homoleptic, four-coordinate azadipyrromethene complexes of d^{10} zinc and mercury. Inorg Chem [Internet]. 2008 Apr 1;47(7):2338–46. Available from: <URL>.

33. Bumagina NA, Krasovskaya ZS, Ksenofontov AA, Antina E V., Berezin MB. Reactivity and zinc affinity of dipyrromethenes as colorimetric sensors: structural and solvation effects. J Mol Liq [Internet]. 2024 Apr 1;399:124397. Available from: <URL>.

34. Helal W, Marashdeh A, Alkhatib Q, Qashmar H, Gharaibeh M, Afaneh AT. Tuning the photophysical properties of BODIPY dyes used in DSSCs as predicted by double-hybrid TD-DFT: The role of the methyl substituents. Int J Quantum Chem [Internet]. 2022 Dec 15;122(24):e27000. Available from: <URL>.

35. Berezin MB, Dogadaeva SA, Antina E V., Lukanov MM, Ksenofontov AA, Semeikin AA. Design and physico-chemical properties of unsymmetrically substituted dipyrromethenes and their complexes with boron(III) and zinc(II). Dye Pigment [Internet]. 2022 Jun 1;202:110215. Available from: <URL>.

36. Bumagina NA, Kritskaya AY, Antina E V., Berezin MB, V'yugin AI. Effect of alkyl, aryl, and meso-aza substitution on the thermal stability of BODIPY. Russ J Inorg Chem [Internet]. 2018 Oct 16;63(10):1326–32. Available from: <URL>.

37. Sevinç G. Photophysical, thermal, and DFT studies on a tetraaryl-azadipyrromethene ligand and its zinc(II) complex. Turkish J Chem [Internet]. 2023 Dec 29;47(6):1438–51. Available from: <URL>.